H1prelim-13-033 Submitted to

XXI International Workshop on Deep-Inelastic Scattering and Related Subjects,
DIS2013, April 22-26, 2013, Marseille Parallel Session **QCD and Final States**

Electronic Access: www-h1.desy.de/publications/H1preliminary.short_list.html

K_s^0 Production at Low Q^2 in Deep-Inelastic ep Scattering at HERA

H1 Collaboration

Abstract

The production of K_s^0 mesons is studied using deep-inelastic events measured with the H1 detector at HERA. The measurements are made in the phase space defined by the negative four-momentum transferred squared of the photon, $7 < Q^2 < 100\,\mathrm{GeV}^2$, and the inelasticity $0.1 < y < 0.6$. Differential K_s^0 production cross sections and ratios of K_s^0 production to charged hadron production are measured. Predictions of leading order Monte Carlo programs are compared to data.

1 Introduction

The measurement of strange particle production in high energy collisions provides valuable information for understanding Quantum Chromodynamics (QCD) in the perturbative and non-perturbative regime. The production of K_s^0, Λ[1] has been studied at different colliders with complementary characteristics; in e^+e^- annihilation at LEP [1–4], in $p\bar{p}$ collisions at Tevatron [6], in pp interactions at RHIC [7], in ep scattering at HERA [8–13] and at the LHC [14–18].

In neutral current deep-inelastic ep scattering (DIS) at HERA the four different processes depicted in figure 1 contribute to strange hadron production. Strange quarks may be created

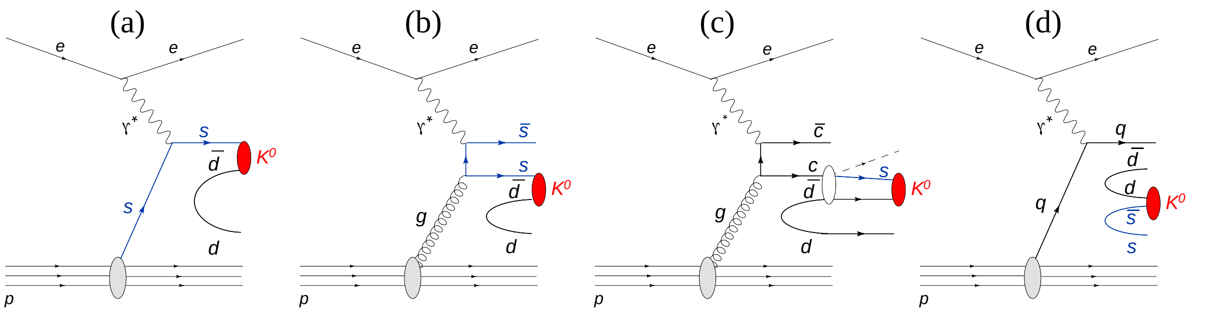

Figure 1: Schematic diagrams for the processes contributing to strangeness production in ep scattering: (a) direct production from the strange sea, (b) BGF, (c) heavy hadron decays and (d) fragmentation. The diagrams relevant for K^0 production are shown.

in the hard sub-process of the ep scattering by originating directly from the strange sea of the proton in a quark-parton-model (QPM) like interaction (figure 1a), from boson-gluon-fusion (BGF, figure 1b) or from the decays of heavy flavoured hadrons (figure 1c). In these production mechanisms hard scales are involved allowing for the applicability of perturbative QCD to be tested. The dominant source for strange hadron production, however, is the creation of an $s\bar{s}$ pairs in the non-perturbative fragmentation process (figure 1d). While strange mesons are created by all four processes strange baryon production receives only little contributions from the decays of heavy flavoured hadrons.

Since s quarks are heavy compared to u and d quarks the formation rate of $s\bar{s}$ pairs in the fragmentation process is expected to be smaller than for $u\bar{u}$ or $d\bar{d}$ pairs. Therefore the production of strange hadrons is expected to be suppressed relative to non-strange hadrons. In the modelling of the fragmentation process this suppression is generally controlled by the strangeness suppression factor λ_s. Especially, the ratio of K_s^0 to charged particles should strongly depend on this quark mass effect.

This paper presents a measurement of K_s^0 production in DIS in the range of negative four momentum transfer squared, $7 < Q^2 < 100\,\mathrm{GeV}^2$ and of lepton inelasticity $0.1 < y < 0.6$. The results are based on a data sample corresponding to an integrated luminosity of $109\,\mathrm{pb}^{-1}$ collected with the H1 detector at HERA at a centre-of-mass energy of $319\,\mathrm{GeV}$ in the years 2006 and 2007. The analysis is performed in a similar kinematic range than covered in previous H1 publications [9, 10, 13]. Results are presented for differential cross sections of K_s^0 production

[1] If not stated differently the charge conjugate state is always implied.

and the ratios of K_s^0 production to charged particles production measured in the same phase space regions. The measurements are shown as a function of various observables characterising the DIS kinematics and the strange particles production dynamics in the laboratory frame. The results are compared with predictions obtained from leading order Monte Carlo calculations, based on matrix elements with parton shower simulation. The rôle of the parton evolution, the strangeness suppression on K_s^0 mesons is investigated.

2 Monte Carlo Simulation

Deep-inelastic ep scattering is modelled using the DJANGH [20] and the RAPGAP [21] programs, which generate hard partonic processes at the Born level at leading order in α_s (e.g. $\gamma * q \to q$, $\gamma * q \to qg$ $\gamma * g \to q\overline{q}$), convoluted with the parton density function (PDF) of the proton. The PDF set CTEQ6L [22] is chosen for this analysis. The factorisation and renormalisation scales a set to $\mu_f^2 = \mu_r^2 = Q^2$. Two different approaches are used for the simulation of higher order QCD effects: in RAPGAP the parton shower approach (MEPS) is implemented in which the parton emission is ordered in transverse momentum (k_T) according to the leading-$\log$ approximation; and in DJANGOH the colour dipol approach (CDM [23]) available within ARIADNE [24] is adopted in which partons are created by colour dipole radiation between the partons in the cascade, resulting in a k_T un-ordered parton emission.

The JETSET program [25] is used for simulating the hadronisation process in the Lund colour string fragmentation model [26]. The suppression of strange quarks is predominantly controlled by a single parameter, $\lambda_s = P_s/P_q$, where P_s and P_q are the probabilities for creating strange (s) or light ($q = u$ or d) quarks in the non-perturbative fragmentation process. The most relevant parameters for describing the baryon production are the di-quark suppression factor $\lambda_{qq} = P_{qq}/P_q$; i.e., the probability of producing a light di-quark pair $qq\overline{qq}$ from the vacuum with respect to a light $q\overline{q}$ pair, and the strange diquark suppression factor $\lambda_{sq} = (P_{sq}/P_{qq})/(P_s/P_q)$, which models the relative production of strange di-quark pairs. The values tuned to hadron production measurements in e^+e^--annihilation by the ALEPH collaboration [5] ($\lambda_s = 0.286, \lambda_{qq} = 0.108$, and $\lambda_{sq} = 0.690$) are taken herein as default values for the simulation of hadronisation within JETSET.

Monte Carlo event samples generated both with DJANGOH and RAPGAP are used for the acceptance and efficiency correction of the data. All generated events are passed through the full GEANT [27] based simulation of the H1 apparatus and are reconstructed and analysed using the same programs as for the data.

3 Experimental Procedure

3.1 The H1 Detector

A detailed description of the H1 detector can be found in [28]. In the following, only those detector components important for the present analysis are described. H1 uses a right handed

Cartesian coordinate system with the origin at the nominal ep interaction point. The proton beam direction defines the positive z-axis of the laboratory frame and transverse momenta are measured in the (x, y) plane. The polar angle θ is measured with respect to this axis and the pseudorapidity η is given by $\eta = -\ln\tan\frac{\theta}{2}$.

Charged particles are measured in the Central Tracking Detector (CTD) in the range $-1.75 < \eta < 1.75$. The CTD comprises two cylindrical Central Jet Chambers (inner CJC1 and outer CJC2), arranged concentrically around the beam-line, complemented by a silicon vertex detector (CST) [29]. The CJCs are separated by a drift chamber which improves the z coordinate reconstruction. A multi-wire proportional chamber mainly used for triggering [30] is situated inside the CJC1. These detectors are arranged concentrically around the interaction region in a solenoidal magnetic field of strength 1.16 T. The trajectories of charged particles are measured with a transverse momentum resolution of $\sigma(p_T)/p_T \simeq 0.2\%\, p_T\,/\,\mathrm{GeV} \oplus 0.015$. In each event the tracks are used in a common fit procedure to determine the ep interaction vertex. The measurement of the specific energy loss dE/dx of charged particles in this detector is known with a resolution of 6.3% for a minimum ionising track [31].

The tracking detectors are surrounded by a Liquid Argon calorimeter (LAr) which measures the positions and energies of particles, including that of the scattered positron, over the polar angle range $4^\circ < \theta < 154^\circ$. The calorimeter consists of an electromagnetic section with lead absorbers and a hadronic section with steel absorbers. The energy resolution for electrons in the electromagnetic section, as measured in beam tests, is $\sigma(E)/E = 11.5\%/\sqrt{E\,[\mathrm{GeV}]} \oplus 1\%$ [32]. In the backward region ($153^\circ < \theta < 178^\circ$), particle energies are measured by a lead-scintillating fibre calorimeter (SpaCal) [33]

The DIS events studied in this paper are triggered by a compact energy deposition in the electromagnetic section of the SpaCal calorimeter. chambers.

The luminosity is determined from the rate of the elastic QED Compton process $ep \to e\gamma p$, with the electron detected in the SpaCal calorimeter, and the rate of DIS events measured in the SpaCal calorimeter [34].

3.2 Selection of DIS Events

The data used in this analysis correspond to an integrated luminosity of $109\ \mathrm{pb}^{-1}$ and were taken by H1 in the years 2006 and 2007 when protons with an energy of 920 GeV collided with electrons[2] with an energy of 27.6 GeV producing a centre-of-mass energy of $\sqrt{s} = 319$ GeV.

The selection of DIS events is based on the identification of the scattered electron as a compact calorimetric deposit in the electromagnetic section of the SpaCal calorimeter in the polar angular range $153^\circ < \theta_e < 173^\circ$, with energy greater than 11 GeV.

At fixed centre-of-mass energies $\sqrt{s}$ the kinematics of the scattering process are described using the Lorentz invariant variables Q^2, y and x. These variables can be expressed as a function of the scattered electron energy E'_e and its scattering angle θ_e in the laboratory frame:

[2]The this paper "electron" is used to denote both electrons and positrons

$$Q^2 = 4E_eE'_e\cos^2\left(\frac{\theta_e}{2}\right), \quad y = 1 - \frac{E'_e}{E_e}\sin^2\left(\frac{\theta_e}{2}\right), \quad x = \frac{Q^2}{ys}. \tag{1}$$

The negative four-momentum transfer squared Q^2 and the inelasticity y are required to lie in the ranges $7 < Q^2 < 100\,\mathrm{GeV}^2$ and $0.1 < y < 0.6$. Background from photo-production events ($Q^2 \approx 0\,\mathrm{GeV}^2$) in which the electron escapes undetected down the beam pipe and a hadron fakes the electron signature, is suppressed by the requirement that the difference $\Sigma(E - p_z)$ between the total energy and the longitudinal momentum must be in the range $35 < \Sigma(E - p_z) < 70\,\mathrm{GeV}$, where the sum includes all measured hadronic final state particles [35] and the scattered electron candidate. The z-coordinate of the event vertex, reconstructed using the tracking detectors, has to be within ± 35 cm of the mean position for ep interactions.

Primary-vertex-fitted charged-particles are selected requiring that the candidates have a minimal radial length of 10 cm and the radial distance from the innermost hit associated with the track to the beam line has to be less than 30 cm. All selected particles have to be in the kinematic region defined by a transverse momentum greater than 500 MeV and the absolute value of their pseudorapidity less than 1.3.

3.3 Selection of K_s^0 Mesons

The K_s^0 mesons are measured by the kinematic reconstruction of its decay $K_s^0 \to \pi^+\pi^-$. The analysis is based on charged particles measured by the CTD with a minimum transverse momentum $p_T \geq 0.12\,\mathrm{GeV}$. The K_s^0 mesons are identified by fitting pairs of oppositely charged tracks in the (x, y) plane to their secondary decay vertices, with the direction of flight of the mother particle constrained to the primary event vertex. Candidates are required to have a minimum radial decay length of 2 cm, a minimum transverse momentum p_T of more than $500\,\mathrm{MeV}$ and to lie in the pseudorapidity range $|\eta| < 1.3$. The phase space of the analysis is summarised in table 1. The contamination from Λ decays is suppressed by rejecting candidates having an invariant mass $M(\pi p) > 1.125\,\mathrm{GeV}$ where the proton hypothesis is assigned to the secondary particle with the larger transverse momentum. The contamination from gamma conversions is suppressed by requiring that the invariant mass, computed under the assumption that the tracks correspond to an electron–positron pair, is bigger than 50 MeV.

DIS kinematics
$7 < Q^2 < 100\,\mathrm{GeV}^2$
$0.1 < y < 0.6$
Hadron kinematics
$0.5 < p_T < 3.5$ GeV
$-1.3 < \eta < 1.3$

Table 1: Analysis phase space

The number of K_s^0 mesons is obtained by fitting the invariant mass spectra with the sum of a signal and background function. For the signal function the t-student function is used while the background distribution is parameterised as

$$B_{K_s^0}(M) = p_0\,(M-2m_T)^{p_1}e^{p_2M+p_3M^2+p_4M^3}, \tag{2}$$
$$\tag{3}$$

Here, M denotes the $\pi^+\pi^-$ invariant mass, and m_T corresponds to the the minimum transverse mass defined as $m_T = \sqrt{m_\pi^2 + (p_{T,min}^{rel})^2}$. For the differential distribution the fit is performed in each kinematic bin.

The invariant mass spectrum $M(\pi^+\pi^-)$ of all candidates passing the selection criteria are shown in figure 2 together with the result from the fits. In total approximately 290000 K_s^0 mesons are reconstructed in the phase space given in table 1. The fitted K_s^0 mass agrees with the world average [36].

4 Cross Sections Determination and Systematic Errors

The total inclusive Born-level cross section σ_{vis} in the kinematic region defined in table 1 is given by the following expression:

$$\sigma_{vis}(ep \to eK_s^0X) = \frac{N}{\mathcal{L}\cdot\epsilon\cdot BR\cdot(1+\delta_{rad})} \quad , \tag{4}$$

where N represents the observed number of K_s^0 mesons and $\mathcal{L}$ and ϵ denote the integrated luminosity and the efficiency, respectively. The branching ratios $BR(K_s^0 \to \pi^+\pi^-)$ is taken from [36]. The radiative corrections $(1+\delta_{rad})$ needed to correct the measured cross section to the Born level are calculated using the program HERACLES [37]. The number of K_s^0 mesons is determined by fitting the mass distribution as explained in section 3.3. In the case of differential distributions the same formula is applied for each analysis bin.

The efficiency ϵ is given by $\epsilon = \epsilon_{rec}\cdot\epsilon_{trig}$, where ϵ_{rec} is the reconstruction efficiency and ϵ_{trig} is the trigger efficiency. The reconstruction efficiency includes the geometric acceptance and the efficiency for track and secondary vertex reconstruction. It is estimated using CDM Monte Carlo event samples. The trigger efficiency is extracted from the data using monitor triggers and is above 99%.

The systematic uncertainties were studied by changing in the Monte Carlo the value of the variables presented below, repeating the analysis procedure and comparing the results to the standard analysis. For the cross section the total uncertainty was calculated adding the different contributions in quadrature, while for the ratios the uncertainties on the energy scale and angle resolution of the scattered electron, as well as on the luminosity, cancel; the other sources are assumed uncorrelated and added in quadrature. For differential distributions the systematic uncertailies are determined in each analysis bin separately. The following sources of systematic uncertainties were considered:

- the uncertainty on the energy scale of the SpaCal calorimeter for scattered electrons,
- the uncertainty of the measurement of the polar angle of the scattered electron,
- the uncertainty on the trigger efficiency,
- the uncertainty on the reconstruction efficiency,
- the uncertainty in the signal extraction due to the two different decay topologies,
- the uncertainty on the extraction of the signal,
- The uncertainty in the correction factor arising from using different Monte Carlo models in the correction procedure, taken as half of the difference between the correction factors obtained with RAPGAP and DJANGO, respectively,
- the uncertainty on the branching ratio (0.5% [36]) and
- the uncertainty in the luminosity measurement.

5 Results and Discussion

5.1 Inclusive Cross Sections

The visible inclusive production cross sections σ_{vis} are measured in the kinematic region defined by $7 < Q^2 < 100\,\mathrm{GeV}^2$ and $0.1 < y < 0.6$ for the event kinematics; and for the kinematics of the neutral strange hadrons, $p_T(K_s^0, \Lambda) > 500\,$MeV, $|\eta(K_s^0, \Lambda)| < 1.3$. A cross sections of:

$$\sigma_{vis}(ep \to eK_s^0 X) = 10.66 \pm 0.02(\text{stat.})^{+0.50}_{-0.53}(\text{syst.})\ \text{nb} \quad (5)$$

is obtained. Using a strangeness suppression factor of $\lambda_s = 0.286$ the models RAPGAP and DJANGOH predict cross sections of 10.93 nb and 9.88 nb, respectively, in reasonable agreement with the measurement.

5.2 Differential cross sections

Differential K_s^0 cross sections are shown in figure 3 as a function the photon virtuality, Q^2, and as a function of the K_s^0 kinematic variables in the laboratory frame, p_T and η along with the predictions of RAPGAP and DJANGOH for a λ_s values of 0.286. The cross sections fall rapidly as Q^2 and p_T grow. The figure also includes the ratios of predicted to measured cross sections for a better shape comparison. Apart from small normalisation differences the models describe the shapes of the measured cross sections as a function of Q^2 and η but predict a significantly softer spectrum in p_T than observed in data.

5.3 Ratio of K_s^0 Production to Charged Particle Production

By normalising the K_s^0 production cross section to the cross section of charged particle production many model dependent uncertainties, like the cross section dependence on proton PDFs, cancel thus enhancing the sensitivity to details of the fragmentation process. In Figure **??** the ratio of K_s^0 production to the cross section charged particle procduction is shown as a function of η, and p_T in comparison to the expectations from DJANGOH using three different values of λ_s ranging from 0.220 to 0.35. The ration in η is well described by the model in shape and a high sensitivity on λ_s is observed in the absolute value of this ratio. However, the shape in p_T is not described. A better understanding of the concurrent processes of K_s^0 production is needed prior to the extraction of the strangeness suppression factor λ_s.

6 Conclusions

This paper presents a study of inclusive K_s^0 production in DIS at low Q^2 measured with the H1 detector at HERA. The kinematic range of the analysis covers the phase space region $7 < Q^2 < 100\,\mathrm{GeV}^2$, and $0.1 < y < 0.6$. The K_s^0 production cross section are measured as a function of the DIS kinematic variable Q^2 and of K_s^0 production variables in the laboratory. In addition results on the ratio of K_s^0 production cross section to the charged particle cross section are presented.

The measurements are compared to model predictions of DJANGOH, based on the colour-dipol model (CDM)and RAPGAP based on DGLAP matrix element calculations supplemented parton showers (MEPS). Within the uncertainties both models provide a reasonable description of the data except for the differential cross section in p_T, where the models predict significantly softer spectra than measured. The sensitivity of the ration of K_s^0 to charged particle production cross sections on the strangeness suppression factor λ_s is demonstrated, however, a better understanding of the concurrent processes of K_s^0 production is mandatory prior to the determination of λ_s.

References

[1] D. Buskulic *et al.* [ALEPH Collaboration], "Production of K0 and Lambda in hadronic Z decays," Z. Phys. **C64**, 361-374 (1994).

[2] M. Acciarri *et al.* [L3 Collaboration], "Measurement of inclusive production of neutral hadrons from Z decays," Phys. Lett. **B328**, 223-233 (1994).

[3] P. Abreu *et al.* [DELPHI Collaboration], "Production characteristics of K0 and light meson resonances in hadronic decays of the Z0," Z. Phys. **C65**, 587-602 (1995).

[4] P. D. Acton *et al.* [OPAL Collaboration], "A Measurement of strange baryon production in hadronic Z0 decays," Phys. Lett. **B291**, 503-518 (1992).

[5] R. Barate *et al.* [ALEPH Collaboration], “Studies of quantum chromodynamics with the ALEPH detector,” Phys. Rept. **294** (1998) 1.

[6] D. Acosta *et al.* [CDF Collaboration], “K_S^0 and Λ^0 production studies in $p\bar{p}$ collisions at $\sqrt{s}$ = 1800-GeV and 630-GeV,” Phys. Rev. **D72**, 052001 (2005). [hep-ex/0504048].

[7] B. I. Abelev *et al.* [STAR Collaboration], “Strange particle production in p+p collisions at s**(1/2) = 200-GeV,” Phys. Rev. **C75**, 064901 (2007). [nucl-ex/0607033].

[8] M. Derrick *et al.* [ZEUS Collaboration], “Neutral strange particle production in deep inelastic scattering at HERA,” Z. Phys. **C68**, 29-42 (1995). [hep-ex/9505011].

[9] S. Aid *et al.* [H1 Collaboration], “Strangeness production in deep inelastic positron - proton scattering at HERA,” Nucl. Phys. **B480**, 3-34 (1996). [hep-ex/9607010].

[10] C. Adloff *et al.* [H1 Collaboration], “Photoproduction of K0 and Lambda at HERA and a comparison with deep inelastic scattering,” Z. Phys. **C76**, 213-221 (1997). [hep-ex/9705018].

[11] J. Breitweg *et al.* [ZEUS Collaboration], “Charged particles and neutral kaons in photo-produced jets at HERA,” Eur. Phys. J. **C2**, 77-93 (1998). [hep-ex/9711018].

[12] S. Chekanov *et al.* [ZEUS Collaboration], “Measurement of K_S^0, Λ, $\bar{\Lambda}$ production at HERA,” Eur. Phys. J. **C51**, 1-23 (2007). [hep-ex/0612023].

[13] F. D. Aaron *et al.* [H1 Collaboration], “Strangeness Production at low Q**2 in Deep-Inelastic ep Scattering at HERA,” Eur. Phys. J. **C61**, 185-205 (2009). [arXiv:0810.4036 [hep-ex]].

[14] K. Aamodt, A. Abrahantes Quintana, D. Adamova, A. M. Adare, M. M. Aggarwal, G. Aglieri Rinella, A. G. Agocs, S. Aguilar Salazar *et al.*, “Strange particle production in proton-proton collisions at sqrt(s) = 0.9 TeV with ALICE at the LHC,” Eur. Phys. J. **C71**, 1594 (2011). [arXiv:1012.3257 [hep-ex]].

[15] V. Khachatryan *et al.* [CMS Collaboration], “Strange Particle Production in pp Collisions at sqrt(s) = 0.9 and 7 TeV,” JHEP **1105**, 064 (2011). [arXiv:1102.4282 [hep-ex]].

[16] RAaij *et al.* [LHCb Collaboration], “Prompt Kshort production in pp collisions at sqrt(s)=0.9 TeV,” Phys. Lett. **B693**, 69-80 (2010). [arXiv:1008.3105 [hep-ex]].

[17] R. Aaij *et al.* [LHCb Collaboration], “Measurement of V^0 production ratios in pp collisions at $\sqrt{s} = 0.9$ and 7 TeV,” JHEP **1108**, 034 (2011). [arXiv:1107.0882 [hep-ex]].

[18] G. Aad *et al.* [ATLAS Collaboration], Phys. Rev. **D 85** (2012) 012001 [arXiv:1111.1297].

[19] R. P. Feynman, “Photon-Hadron-Interactions”, Benjamin, New York (1972).

[20] G. A. Schuler and H. Siesberger, DJANGO, Proceedings of “Physics at HERA”, eds. W. Buchmüller and G. Ingelman, DESY, Hamburg (1992) 1419.

[21] H. Jung, “Hard diffractive scattering in high-energy e p collisions and the Monte Carlo generator RAPGAP,” Comp. Phys. Commun. 86 (1995) 147.

[22] J. Pumplin *et al.*, JHEP **0207** (2002) 012, [hep-ph/0201195].

[23] B. Andersson *et al.* “Coherence Effects in Deep Inelastic Scattering,” Z. Phys. C **43** (1989) 625;
L. Lönnblad, “Rapidity gaps and other final state properties in the colour dipole model for deep inelastic scattering,” Z. Phys. C **65** (1995) 285.

[24] L. Lönnblad, “Ariadne Version 4: A Program For Simulation Of QCD Cascades Implementing The Colour Dipole Model,” Ariadne version 4, Comput. Phys. Commun. **71** (1992) 15.

[25] T. Sjöstrand, “High-energy physics event generation with PYTHIA 5.7 and JETSET 7.4,” Comput. Phys. Commun. **82** (1994) 74, JETSET version 7.4 is used.

[26] T. Sjöstrand, “The Lund Monte Carlo For Jet Fragmentation And E+ E- Physics: Jetset Version 6.2,” Comput. Phys. Commun. **39** (1986) 347;
T. Sjöstrand and M. Bengtsson, “The Lund Monte Carlo For Jet Fragmentation And E+ E- Physics. Jetset Version 6.3: An Update,” Comput. Phys. Commun. **43** (1987) 367;
B. Andersson *et al.* “Parton Fragmentation And String Dynamics,” Phys. Rept. **97** (1983) 31.

[27] R. Brun *et al.* GEANT3, Technical Report CERN-DD/EE/84-1, CERN, 1987.

[28] I. Abt *et al.* [H1 Collaboration], “The H1 detector at HERA,” Nucl. Instrum. Meth. A **386** (1997) 310;
I. Abt *et al.* [H1 Collaboration], “The Tracking, calorimeter and muon detectors of the H1 experiment at HERA,” Nucl. Instrum. Meth. A **386** (1997) 348.

[29] D. Pitzl *et al.*, “The H1 silicon vertex detector,” Nucl. Instrum. Meth. A **454** (2000) 334 [hep-ex/0002044].

[30] J. Becker *et al.*, “A Vertex Trigger based on Cylindrical Multiwire Proportional Chambers” Nucl. Instrum. Meth. A **586** (2008) 190, [physics/0701002].

[31] E. Hennekemper, “Simulation and Calibration of the Specific Energy Loss of the Central Jet Chambers of the H1 Detector and Measurement of the Inclusive D^* Meson Cross Section in Photoproduction at HERA”, Ph.D. thesis, Univ. Heidelberg (2011), HD-KIP-11-68 (available at http://www-h1.desy.de/publications/thesis_list.html).

[32] B. Andrieu *et al.* [H1 Calorimeter Group], “Beam tests and calibration of the H1 liquid argon calorimeter with electrons,” Nucl. Instrum. Meth. A **350** (1994) 57.

[33] R.D. Appuhn *et al.*, “The H1 lead/scintillating-fibre calorimeter,” Nucl. Instrum. Meth. A **386** (1997) 397.

[34] F.D. Aaron *et al.* [H1 Collaboration], “Determination of the Integrated Luminosity at HERA using Elastic QED Compton Events”, Eur. Phys J. **C72** (2012) 2163, [arXiv:1205.2448].

[35] M. Peez, 'Recherche de déviations au Modèle Standard dans les processus de grande énergie transverse sur le collisionneur électron-proton HERA', PhD thesis (in French), Université de Lyon (2003), DESY-THESIS-2003-023
available at http://www-h1.desy.de/publications/theses_list.html;
S. Hellwig, 'Untersuchung der D^*-π_{slow} Double Tagging Methode in Charmanalysen', Dipl. thesis (in German), Univ. Hamburg (2004)
available at http://www-h1.desy.de/publications/theses_list.html.

[36] K. Nakamura et al. (Particle Data Group), J. Phys. G 37, 075021 (2010).

[37] A. Kwiatkowski, H. Spiesberger and H. J. Möhring, "HERACLES: An Event Generator for e p Interactionsat HERA Energies including Radiative Processes: Version 1.0," HERACLES version 1.0, Comput. Phys. Commun. **69** (1992) 155.

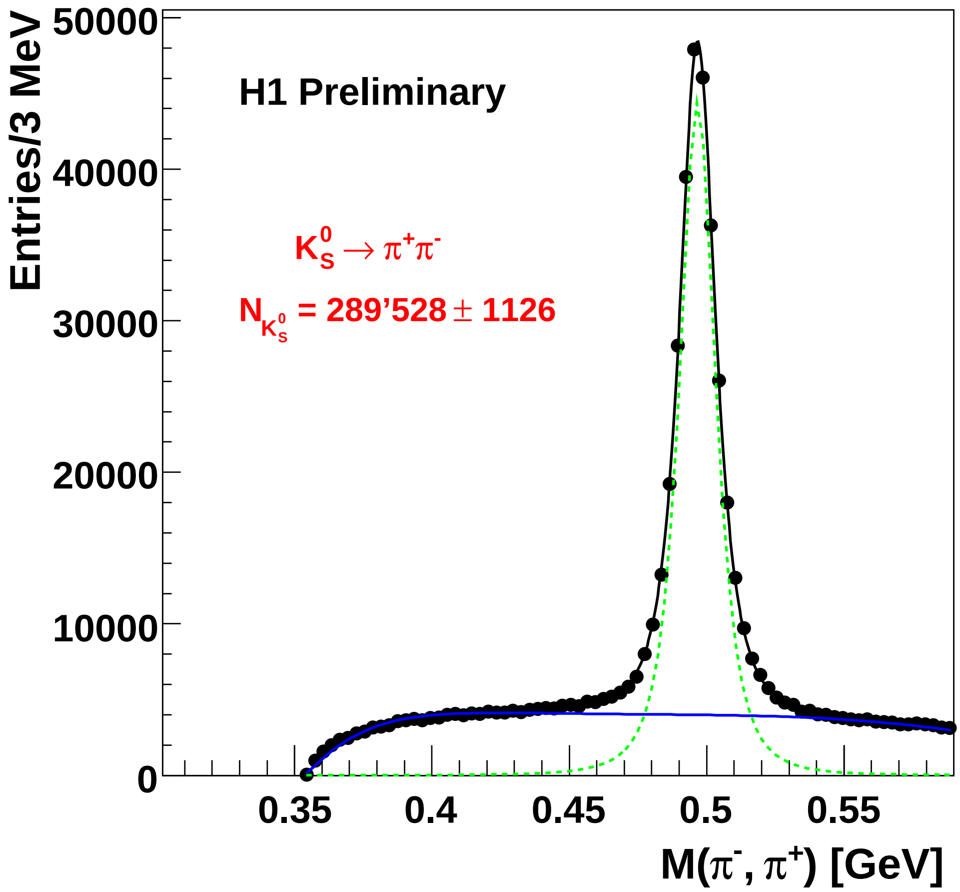

Figure 2: Mass distributions for K_s^0 candidates.

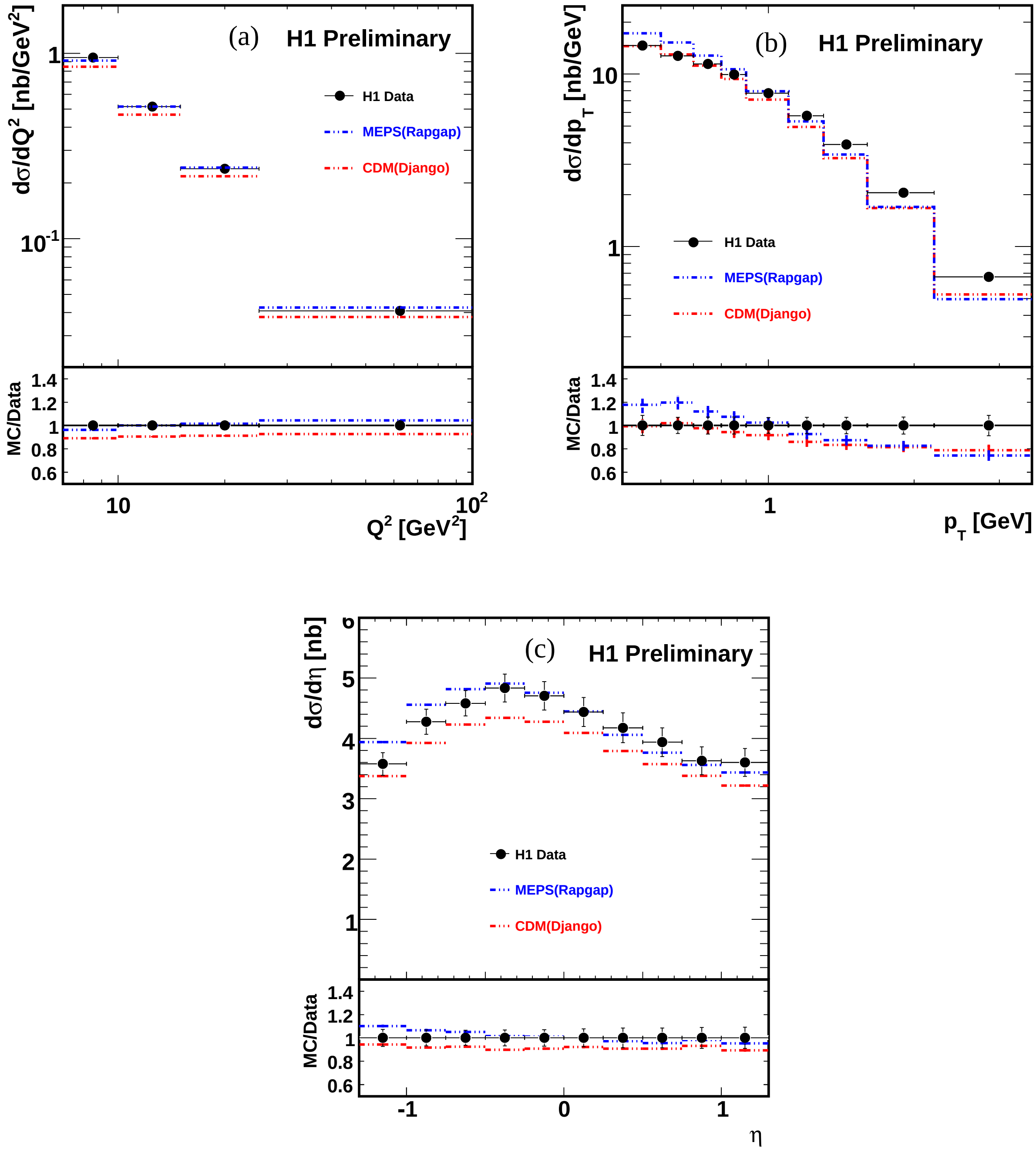

Figure 3: Differential K_s^0 production cross sections as a function of (a) the photon virtuality squared Q^2, (b) the transverse momentum, p_T, of the Λ baryon and (c) its pseudorapidity η in comparison to RAPGAP (MEPS) and DJANGOH (CDM). The inner (outer) error bars show the statistical (total) errors. The ratios "MC/Data" are shown for the different Monte Carlo predictions. For comparison, the data points are put to one.

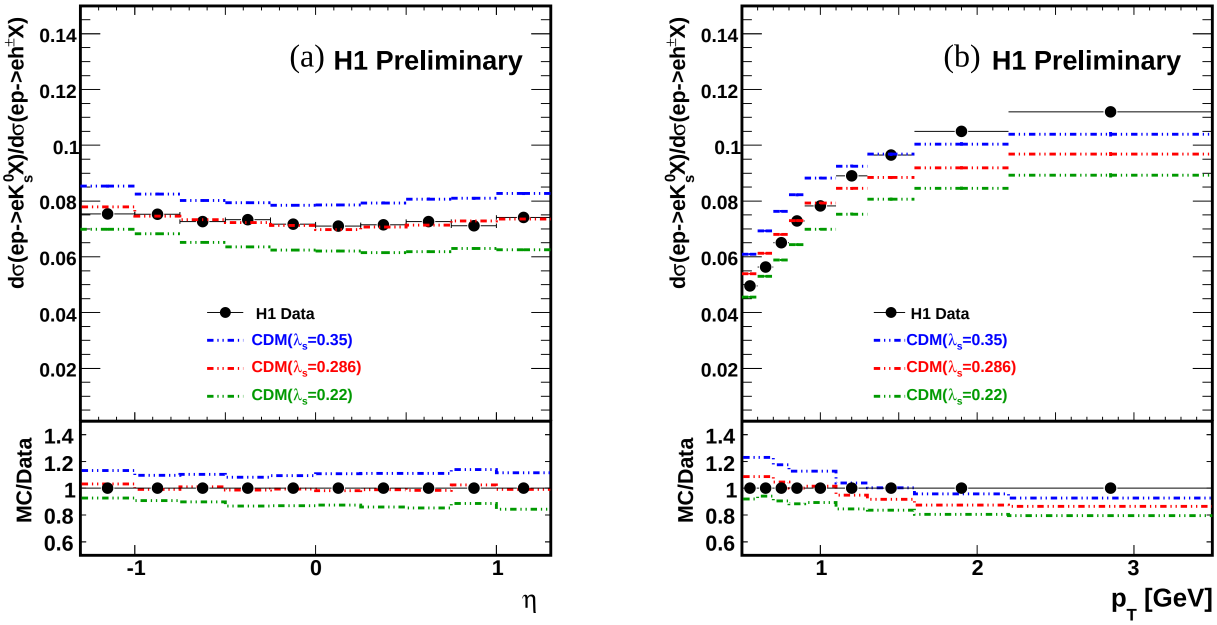

Figure 4: Ratio of K_s^0 to charged particle production as a function of (a) η and (b) p_T, in comparison to DJANGOH (CDM) for three different vaues of λ_s. The inner (outer) error bars show the statistical (total) errors. The ratios "MC/Data" are shown for the different Monte Carlo predictions. For the ratios the data points are put at one for comparison.